IEEE Access
Multidisciplinary ⋮ Rapid Review ⋮ Open Access Journal

Received 8 March 2024, accepted 22 March 2024, date of publication 8 April 2024, date of current version 26 April 2024.

Digital Object Identifier 10.1109/ACCESS.2024.3386366

APPLIED RESEARCH

A Hierarchical Optimizing Energy Management Strategy for Alleviating Degradation in Fuel Cell Hybrid System

JUN FU[1], QIAN XIANG[1], LINGHONG ZENG[1], YANMIN ZU[1,2], HANG YOU[1], XINKAI SHAN[1], JIE XIN[3], AND XI LI[1], (Member, IEEE)

[1]School of Artificial Intelligence and Automation, Key Laboratory of Image Processing and Intelligent Control of Education Ministry, Huazhong University of Science and Technology, Wuhan 430074, China
[2]State Grid Corporation of China, Beijing 102200, China
[3]Hangzhou ArcSoft Software Company Ltd., Hangzhou 310051, China

Corresponding author: Xi Li (lixi@hust.edu.cn)

This work was supported in part by the National Natural Science Foundation of China under Grant U2066202 and Grant 2022YFB4002200; and in part by the Science, Technology and Innovation Commission of Shenzhen Municipality under Grant JCYJ20210324115606017.

ABSTRACT This study designs an energy management strategy for fuel cell hybrid vehicles aimed to alleviating the performance degradation of Proton Exchange Membrane Fuel Cells (PEMFC), fuel consumption, and battery State of Charge (SOC) fluctuations during vehicle operation. The research focuses on the decrease in Electrochemical Surface Area (ECSA) due to Platinum (Pt) catalyst degradation, which is a key factor influencing PEMFC durability. An ECSA model based on the Pt dissolution mechanism is established, and a dynamic condition accelerated stress test (DC-AST) is designed to specifically investigate the impacts of key parameters, such as cycle period, amplitude, and duty cycle on the degradation of ECSA. This reveals the association between ECSA degradation and irregular potential fluctuations. A hierarchical power allocation strategy is then proposed, combining the global search capabilities of optimization algorithms with heuristic strategies in light of these features. The upper level employs Pontryagin's Minimum Principle (PMP) strategy for global power allocation optimization, while the lower level uses a satisfaction-based heuristic strategy that is tailored to the ECSA degradation characteristics, to dynamically adjust power output. Simulation results demonstrate that, compared to traditional rule-based strategies and classical PMP-based strategies, the proposed energy management strategy more effectively mitigates ECSA degradation of PEMFC under typical vehicle conditions.

INDEX TERMS PEMFC, hybrid power, degradation, ECSA, energy management.

I. INTRODUCTION

The massive consumption of fossil fuels has led to worldwide energy and environmental crises. With low pollution, high efficiency, and fast start-up, proton exchange membrane fuel cells (PEMFCs) are considered to be the most promising clean alternative energy source for vehicles [1]. However, great challenges in cost and durability are still limiting its commercialization. Therefore, it is crucial to mitigate PEMFC degradation under vehicle operating conditions [2].

The associate editor coordinating the review of this manuscript and approving it for publication was Qiang Li.

Optimizing power allocation among energy sources is crucial for enhancing the durability of fuel cell hybrid vehicles, and various strategies that consider performance degradation have been proposed. Song et al. [3] established a fuel cell health state model to adaptively adjust power allocation according to the degradation state of the fuel cell system. Goshtasbi [4] proposed a linear time-varying model predictive control framework to constrain the operating conditions. Zhou et al. [5] used internal resistance and limit current to characterize the degradation of fuel cells and then used a twisting control algorithm according to the degradation state. Reference [6] divided the factors affecting fuel cell

degradation into four typical operating conditions and then proposed an optimal control method based on the system's efficiency and degradation cost. Li et al. [7] has developed an internal resistance degradation model whereby the hydrogen consumption equivalent factor is adapted according to the state of health (SOH). Kwon et al. [8] defined the degradation rate of a fuel cell through the deviation between output and rated power and then converted it into equivalent hydrogen consumption as the optimization objective. Li et al. [9] developed a fuel cell lifetime model that accounts for cyclic load fluctuations. Zhou et.al. [10] employed the duration time of four typical operating conditions to characterize the degradation and turned it into degradation cost. Reference [11] indirectly characterizes the fuel cell performance degradation via power fluctuations and integrates it into objective function.

In the literature reviewed, two methods have been utilized to quantify performance degradation. The first involves constructing a degradation model that typically incorporates electrical parameters—such as voltage, current, internal resistance, or output power—as indicators of degradation. The second method indirectly assesses fuel cell degradation under various typical operating conditions, with only a few variables directly representing degradation based on fundamental principles. Within power splitting strategies, the traditional methodology either directly or indirectly incorporates these degradation indicators into the objective function, which is then minimized to determine the optimal power allocation.

Numerous factors influence the durability of PEMFCs. During actual vehicle operation, frequent load changes can cause electrode potential fluctuations, which may accelerate the degradation of platinum (Pt) catalysts. Reference [12] suggests that this degradation, resulting in a diminished electrochemical active surface area (ECSA), constitutes the primary cause of stack performance degradation.

This paper adopts a control method based on surrogate parameters to indirectly manage the degradation of the ECSA in fuel cells through the adjustment of macro-level voltage parameters. Considering the degradation characteristics of ECSA, a Hierarchical Power Allocation Strategy (HPAS-D) is designed, which integrates heuristic rules with the global search capabilities of optimization algorithms. This strategy optimizes power allocation at the global level using Pontryagin's Minimum Principle (PMP) algorithm, while simultaneously conducting fine-tuned adjustments to the output power at the local level based on the degradation characteristics of ECSA. The approach effectively mitigates the degradation of ECSA and maintains the stability of the State of Charge (SOC).

This study investigates the dissolution mechanism of platinum in the catalytic layer (CL) under vehicular driving conditions. It establishes an ECSA degradation model based on platinum dissolution. To assess ECSA degradation characteristics, a Dynamic Condition Accelerated Stress Test (DC-AST) was developed. Furthermore, leveraging these characteristics, the study designs a heuristic strategy. It integrated with the classical Pontryagin's Minimum Principle (PMP) optimization method and forms a hierarchical power allocation approach. Additionally, this research employs ECSA degradation as a metric to quantitatively assess the effectiveness of Energy Management Strategies (EMS) in mitigating fuel cell degradation.

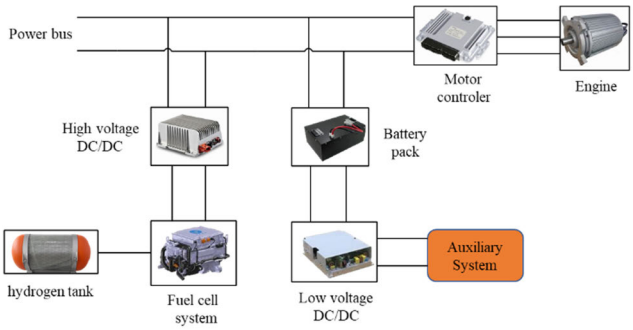

FIGURE 1. Hybrid power system structure.

TABLE 1. Vehicle and powertrain parameters.

Category	Item	Value
Vehicle parameters	Vehicle total mass (kg)	1577
	Wheel radius (m)	0.31
	Aerodynamic drag coefficient	0.33
	Vehicle frontal area (m^2)	2.254
	Air density (kg/m^3)	1.21
	Rolling coefficient	0.013
	drive efficiency	0.945
PEMFC system	Rated power (kW)	40
Lithium-ion Battery Pack	capacity (Ah)	20
	Open circuit voltage (V)	350
Electric motor	Rated power (kW)	75

II. POWERTRAIN STRUCTURE DESCRIPTION AND MODEL

A. POWDERTRAIN DESCRIPTION

This study takes a medium-sized series hybrid electric vehicle (HEV) as the research object, with a PEMFC system serving as the primary power source. The powertrain mainly comprises a PEMFC system, battery, DC/DC converter, DC engine, etc. Fig.1 illustrates the structure of the HEV powertrain [12].

The powertrain can operate in four basic working modes: fuel cell driving, battery driving, hybrid, and regenerative braking. The parameters are listed in Table 1.

B. FUEL CELL SYSTEM

The PEMFC system comprises a fuel cell stack and an auxiliary system.

1) VOLTAGE MODEL

The actual output voltage of the fuel cell is determined by subtracting the overvoltage loss from the thermodynamic predicted voltage.

$$v_{fc} = E_{nernst} - v_{act} - v_{ohm} - v_{conc} \tag{1}$$

Here, E_{nernst} is the theoretical open-circuit voltage. v_{act}, v_{ohm} and v_{conc} represent activation loss, ohmic loss, and concentration loss, respectively. They can be described by mechanisms or empirical equations.

$$E_{nernst} = 1.229 - 0.85 \times 10^{-3}\left(T_{fc} - 298.15\right) + 4.3085 \times 10^{-5} T_{fc}\left[\ln\left(p_{H_2}\right) + \frac{1}{2}\ln\left(p_{Q_2}\right)\right] \quad (2)$$

$$v_{act} = \alpha \ln\left(\frac{i}{i_0}\right) \quad (3)$$

$$v_{ohm} = i \cdot R_{ohm} \quad (4)$$

$$v_{conc} = -\beta_e \frac{RT}{4F} \ln\left(1 - \frac{i}{i_{lim}}\right) \quad (5)$$

where T_{fc} is the working temperature of the stack, p_{H_2}, p_{Q_2} is the partial pressure of the hydrogen, and oxygen, i is the current density, i_0 is the exchange current density, R_{ohm} is the equivalent internal resistance of the fuel cell, β_e is an empirical parameter, i_{lim} is the limit current density, and α is a constant.

2) HYDROGEN CONSUMPTION

Hydrogen consumption during operation is given by:

$$m_{H_2} = \int_0^t \frac{P_{fc}(\tau)}{\eta_{fcs} \cdot LHV_{H_2}} d\tau \quad (6)$$

where m_{H_2} is the mass consumption of hydrogen, η_{fcs} is the efficiency of the PEMFC system, and LHV_{H_2} is the low calorific value of H_2.

C. BATTERY MODEL

Batteries serve as both an auxiliary power source and an energy storage device, supplying additional electric power and recovering regenerative braking energy.

The open-circuit voltage (OCV) of a battery is related to the state of charge (SOC) and temperature. In this study, it is assumed that the battery parameters remain constant with temperature changes. Therefore, the DC bus voltage of a single battery can be expressed as:

$$V_{bat} = V_{oc}(SOC) - I_{bat} \cdot R_{int}(SOC) \quad (7)$$

where V_{oc} represents the open-circuit voltage, and R_{int} denotes the internal resistance of the battery.

The state of charge (SOC) is a crucial parameter for describing the working state of a battery. It can be described as:

$$SOC(t) = SOC_0 - \int_0^t \frac{\eta_{bat} \cdot I_{bat}(\tau)}{Q_{bat}} d\tau \quad (8)$$

where SOC_0 is the initial SOC, η_{bat} is the battery's efficiency, and Q_{bat} is the battery's nominal capacity.

III. DEGRADATION MODEL

The degradation of fuel cell performance significantly influences their service life. This section describes the dissolution mechanism of Pt catalysts and develops a degradation model.

A. DEGRADATION MECHANISM

Platinum is chemically stable and does not react under normal conditions. Nevertheless, Pt is unstable in typical PEMFC operating environments. Oxidation processes are prone to occur on the platinum surface during PEMFC operation, resulting in platinum dissolution and loss [13], [14].

Studies reveal that the potential cycle is the primary factor leading to platinum dissolution. In potential cycle, reactions such as electrochemical dissolution, oxidation, chemical dissolution, and reduction of Pt co-occur on the Pt particle surface. The platinum dissolution and deposition process may occur through the following steps [15], [16].

1) POTENTIAL RISE

When the potential reaches approximately 0.6 V, some oxides begin forming on the surface of the Pt cluster.

$$Pt + H_2O \rightarrow PtO + 2H^+ + 2e^- \quad Reaction\ (1)$$

The exposed region loses electrons under the potential, oxidizes to Pt ions, and diffuses, corresponding to electrochemical dissolution.

$$Pt \rightarrow Pt^{2+} + 2e^- \quad Reaction\ (2)$$

Pt dissolution becomes evident when the potential exceeds 0.8V, and the dissolution rate increases as the potential rises [17]. At high potential (>1.2 V), the platinum catalyst surface is covered with an oxide layer, which isolates Pt particles and inhibits dissolution [17], [18].

2) POTENTIAL DROP

As the potential decreases, Pt ions dissolved are then reduced by H_2 permeating from the anode, deposited on other Pt clusters, changing the catalyst's morphology and resulting in a decline in catalyst activity. The deposit process of Pt ions in the membrane is considered irreversible [19].

$$Pt^{2+} + H_2 \rightarrow Pt + 2H^+ \quad Reaction\ (3)$$

The chemical dissolution of PtO reduces the oxide film on the platinum surface and exposes the metallic platinum. This corresponds to reaction (4), which is relatively slow.

$$PtO + 2H^+ \rightarrow Pt^{2+} + H_2O \quad Reaction\ (4)$$

At low potentials below 0.6 V, reactions (1), (2), and (4) occur slowly, and the platinum dissolution is almost negligible.

Simplifying the above process, we may combine reactions (1) and (4) and consider reaction (3) to be the reverse reaction of reaction (2). Therefore, the following reactions were obtained [20]:

$$Pt \leftrightarrow Pt^{2+} + 2e^- \quad Reaction\ 1$$

$$Pt + H_2O \leftrightarrow PtO + 2H^+ + 2e^- \quad Reaction\ 2$$

At high potential, where the forward reaction rate $\gg$ reverse reaction rate and Pt cluster dissolution occurs. At low potential, the reverse reaction rate $\gg$ forward reaction rate,

reactions 1 and 2 reverse reactions occur, and the Pt ions dissolved in the surrounding area are reduced to Pt particles and redeposited.

During the continuous dissolution and redeposition process, platinum is lost and redistributed, and the effective surface area of the catalyst decreases, resulting in catalyst deterioration [21], [22], [23].

B. ECSA DEGRADATION MODEL

According to subsection A, the kinetics of the two processes above may be determined using the following equations [18], [20], [24]:

$$v_1 = (1-\theta)\, k_1 exp\left(\frac{1}{r}\frac{\beta_\gamma V_{Pt}}{RT}\right) \times exp\left\{\frac{F}{RT}\left(E - E_1^{eq} + \frac{1}{r}\frac{2\beta_\gamma V_{Pt}}{F}\right)\right\} \tag{9}$$

$$v_{-1} = (1-\theta)\, k_{-1} exp\left(\frac{1}{r}\frac{\beta_\gamma V_{Pt}}{RT}\right) \times exp\left\{-\frac{F}{RT}\left(E - E_1^{eq} + \frac{1}{r}\frac{2\beta_\gamma V_{Pt}}{F}\right)\right\}\left(\frac{c_{Pt}}{c_{Pt}^{ref}}\right) \tag{10}$$

$$v_2 = k_2 exp\left(\frac{1}{r}\frac{\beta_\gamma V_{Pt}}{RT}\right) exp\left(-\frac{\omega}{RT}\theta\right) \times exp\left\{\frac{F}{RT}\left(E - E_2^{eq}\right)\right\} \tag{11}$$

$$v_{-2} = k_{-2} exp\left(\frac{1}{r}\frac{\beta_\gamma V_{Pt}}{RT}\right)\theta exp\left\{-\frac{F}{RT}\left(E - E_2^{eq}\right)\right\} \tag{12}$$

where c_{Pt} is the Pt ion concentration, E_1^{eq} and E_2^{eq} is the equilibrium potential, d_0 is the initial average of particle diameter, k_1, k_{-1}, k_2, k_{-2} is the rate constant of Pt dissolution and deposition, P_tO formation and reduction, v_1, v_{-1}, v_2, and v_{-2} represent their rate respectively. V_{Pt} is the Pt molar volume, β_γ is surface tension, Γ_{max} is the number of adsorption sites, ε represents the vacancy rate, and ω is the interfacial surface tension.

Then, the platinum particle size is calculated by the following equation:

$$\Delta r = -V_{Pt}\,(v_1 - v_{-1})\,\Delta t \tag{13}$$

$$\Delta\theta = \left(\frac{1}{\Gamma_{max}}(v_2 - v_{-2}) + \frac{2\theta V_{Pt}}{r}(v_1 - v_{-1})\right)\Delta t \tag{14}$$

$$\Delta c_{Pt} = \frac{4\pi r^2 N}{\varepsilon}(v_1 - v_{-1})\,\Delta t \tag{15}$$

where Δr is the particle size change rate, r is the Pt cluster diameter, and N is the number of Pt particles per volume.

ECSA is defined as the surface area per unit mass of the platinum cluster. Assume that the Pt cluster is a perfect sphere. Therefore, the ECSA value at time t may be calculated:

$$ECSA\,(t) = \frac{\sum_i 4\pi r_i^2}{\rho \sum_i \frac{4}{3}\pi r_i^3} = \frac{3\sum_i r_i^2}{\rho \sum_i r_i^3} \tag{16}$$

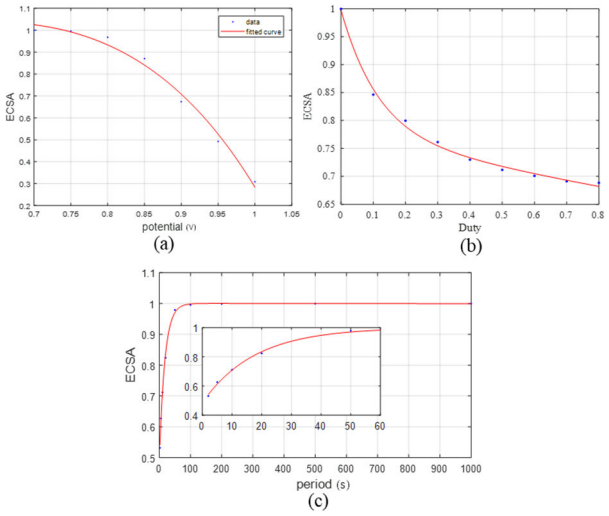

FIGURE 2. DC-AST test of the ECSA model: (a) Relationship between ECSA decay and high potentials; (b) ECSA decay versus AST cycle time; (c) Relationship between ECSA decay and duty cycle.

where ρ represents the platinum density, and r_i represents the particle radius.

Employing accelerated stress testing (AST), the model underwent validation under conditions analogous to those delineated in Reference [17]. The observed trends in Pt particle size and ECSA decay aligned with the findings reported in the aforementioned reference.

C. DEGRADATION CHARACTERISTIC ANALYSIS

To examine the influence of vehicle operating conditions on ECSA, a dynamic condition accelerated stress test (DC-AST) was developed. The test simulates potential fluctuations in fuel cell electrodes under operating conditions and aims to explore the degradation characteristics of ECSA under various potentials. The experiment employed square waveforms, commonly used signals for accelerated aging, to specifically examine the effects of key parameters, including cycle period, amplitude, and duty cycle, on ECSA degradation. By adjusting the waveform period to simulate the rate of load variations and modifying the voltage amplitude to reflect different operating states, the study also considers the influence of the duty cycle.

Assuming all tests are conducted at room temperature, the variations in ECSA values under differing cycle periods, amplitudes, and duty cycles are systematically tested and documented based on the model, employing the controlled variable method. Subsequently, corresponding patterns are summarized.

1) HIGH POTENTIAL TEST

The test conditions are as follows: a square with a low level of 0.6 V, a duty cycle of 50%, and a period of 10 seconds (s). Give a range of high voltages between 0.6 and 0.95 V with an iteration period of 7×10^6 seconds, which corresponds to

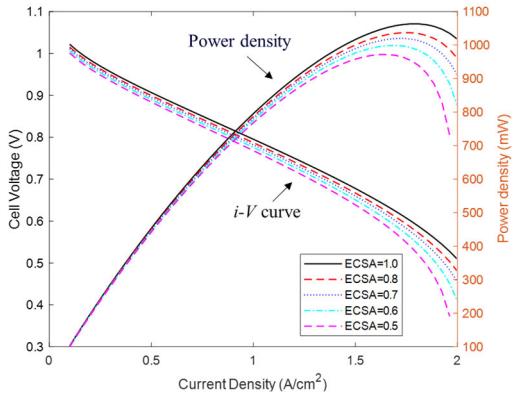

FIGURE 3. Polarization curves during the durability test.

an ECSA attenuation of about 50%. The normalized ECSA attenuation is shown in Fig. 2(a).

2) DUTY CYCLE TEST

The test conditions are as follows: a square wave period of 10 s, with a potential range from 0.6 to 0.95 V, and the number of iterations is 100,000.

3) PERIODIC TESTING

The voltage range is 0.6 V to 0.95 V, with a 50% duty cycle, and the period from 2 to 1000 s. Each period performed 100000 cycles. The fitted curve is shown in Fig. 2(c).

Test results delineate the decay characteristics of the ECSA as follows: (i) Within a potential range of 0.6 V to 1.1 V, there is a positive correlation between the ECSA decay rate and the potential. (ii) For duty cycles of the AST below 90%, the ECSA decay rate escalates with an increase in duty cycle, given constant period and iteration counts. (iii) An inverse relationship is observed between the ECSA decay rate and the AST period, with a notable reduction in the decay rate when the period extends beyond 20 seconds.

The aforementioned results can inform power regulation strategies for PEMFCs in hybrid systems. The fuel cells should avoid operating under unfavorable conditions and the test results may be used as a reference for quantitative adjustment.

4) PERFORMANCE TEST

The principal features of fuel cell degradation are diminished power output and voltage decline. To assess the influence of ECSA degradation on fuel cell performance, polarization curves and power characteristics were evaluated under varying ECSA conditions. Fig. 3 presents the polarization and power-current curves, facilitating an analysis of performance across the entire operational range.

The figure demonstrates that the rate of degradation varies across different current densities. Notably, the voltage remains relatively stable at low current densities but decreases more rapidly at higher currents. When the current density is higher than approximately 1500 mA/cm-2, the performance of the PEMFC experiences a dramatically drop.

TABLE 2. Rule-based power allocation strategy.

SOC	$P_{req} < P_{min}$	$P_{min} < P_{req} < P_\eta$	$P_\eta < P_{req} < P_{max}$	$P_{req} > P_{max}$
<0.3	$P_{fc} = P_\eta$	$P_{fc} = P_\eta$	$P_{fc} = P_{max}$	$P_{fc} = P_{max}$
0.3~0.8	$P_{fc} = P_{max}$	$P_{fc} = P_\eta$	$P_{fc} = P_\eta$	$P_{fc} = P_{max}$
>0.8	$P_{fc} = P_{min}$	$P_{fc} = P_{min}$	$P_{fc} = P_\eta$	$P_{fc} = P_{max}$

The result suggests that kinetic, ohmic, and mass transfer losses increase when ECSA decreases. At high current density, the microscale transmission resistance dominates the voltage loss in catalytic layer, the ECSA loss significantly magnifies the microscale transfer resistance [25]. Undervoltage at high current densities indicates that PEMFC output power is insufficient at high power demand. Therefore, it is necessary to quantitatively estimate the ECSA decay of PEMFC and adopt mitigation strategies to suppress ECSA degradation under dynamic load conditions.

IV. ENERGY MANAGEMENT

The energy management strategy (EMS) for a fuel cell hybrid system aims to allocate power demand properly among the sources. This section proposes a hybrid strategy that integrates optimization and rule-based approaches.

A. RULE-BASED ENERGY MANAGEMENT STRATEGY

The following principles should be considered while designing the controller:

(i) The fuel cell should provide energy when load demands are relatively low, while both the fuel cell and the battery should share the power demands under heavy loads.

(ii) It is essential to maintain a relatively stable output voltage from the fuel cell.

(iii) The SOC of the battery should be kept within a specific range to avoid overcharging or over-discharging.

This strategy divides the fuel cell operating power into several sections, takes into account power demand and battery SOC, and focuses on the FC operating in the efficiency area.

Battery's SOC application range significantly influences its performance and service life. It is necessary to comprehensively weigh each influencing factor to obtain an optimized solution for SOC operating range [17]. Considering safety, energy demand, efficiency range and battery life, the SOC service range is chosen at 30%-80%.

During operation, the energy allocation strategy considers the battery's state of charge and dynamically adjusts the fuel cell's output based on current power demand. The specific power allocation rules are designed as outlined in Table 2. In Table 2, where P_{fc} denotes the fuel cell output power, P_{req} represents the real-time power demand, P_{min} and P_{max} respectively indicate the minimum and maximum output power of the fuel cell, and P_η refers to the output power at

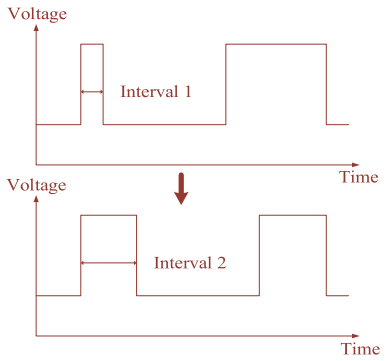

FIGURE 4. Illustration of the strategy.

the fuel cell's optimal efficiency point. Simulation results are discussed in next Section.

B. PMP-BASED ENERGY MANAGEMENT STRATEGY

PMP-based optimization in energy allocation strategies results in solutions close to the global optimum under specific conditions [27]. To improve fuel efficiency, hydrogen consumption is defined as the system's objective function.

$$J_{min} = min\left(\int_{t_0}^{t_f} \dot{m}\left[P_{fc}\left(t\right), t\right] dt\right) \tag{17}$$

where t_0, t_f represents the initial and final time of the driving cycle.

Construct the Hamiltonian function with battery SOC as the state variable and the PEMFC output power as control variable.

$$H\left(x, u, \lambda, t\right) = \dot{m}_H\left(P_{fc}\left(t\right), t\right) + \lambda\left(t\right) S\dot{O}C\left(t\right) \tag{18}$$

where $\dot{m}_H$ is the hydrogen consumption rate, λ is the costate variable.

According to the PMP principle, to minimize the performance index J, there must be an optimum control variable that minimizes the Hamiltonian function [3].

$$H\left(x^*, u^*, \lambda^*\right) = \min_{u \in U} H\left(x^*\left(t\right), u\left(t\right), \lambda^*\left(t\right)\right) \tag{19}$$

where $x\left(t\right)$ is the state variable, $u\left(t\right)$ is the control variable.

The optimal state variable $x\left(t\right)$ and the costate variable $\lambda\left(t\right)$ need to meet the system canonical equation:

$$\begin{cases} \dot{x}(t) = \dfrac{\partial H\left(x\left(t\right), P_{fc}^*\left(t\right), t\right)}{\partial \lambda\left(t\right)} \\ \dot{\lambda}(t) = -\dfrac{\partial H\left(x\left(t\right), P_{fc}^*\left(t\right), t\right)}{\partial x\left(t\right)} \end{cases} \tag{20}$$

The constraints are set as follows:

$$\begin{cases} P_{fc,min} \leqslant P_{fc} \leqslant P_{fc,max} \\ P_{bat,min} \leqslant P_{bat} \leqslant P_{bat,max} \\ SOC_{min} \leqslant SOC \leqslant SOC_{max} \end{cases} \tag{21}$$

Assumed:

$$SOC\left(t_0\right) = SOC\left(t_f\right) \tag{22}$$

the variables t_0 and t_f are interpreted as in equation (34).

The optimal control trajectory u*(t) can then be obtained by finding the minimum value of the Hamilton function at each sampling time:

$$P_{fc}^*(t) = \arg minH\left[P_{fc}\left(t\right), SOC\left(t\right), \lambda\left(t\right)\right] \tag{23}$$

C. HIERARCHICAL POWER ALLOCATION STRATEGY BASED ON DEGRADATION CHARACTERISTICS

Section III presents an ECSA model and derives meaningful degradation characteristics from the DC-AST test. This section proposes a hierarchical power allocation strategy based on the degradation characteristics, termed HPAS-D, which integrates optimization algorithms with heuristic-based strategies to combine their respective advantages. The upper layer distributes power using PMP control, while the lower layer modulates dynamic power fluctuation using a Satisfaction-Based Dynamic Fluctuation Adjustment (S_DFA) strategy based on ECSA degradation characteristics.

The majority of studies aim to reduce swings in power amplitude. This strategy considers not only the amplitude but also the fluctuation interval. Fig. 4 illustrates that, despite both voltage waveforms exhibiting identical total output power in terms of amplitude, Section III reveals that the power fluctuations, as depicted in the lower subfigure, contribute to a slower degradation of the electrochemical surface area.

ECSA degradation commonly arises during the transition between high and low potentials due to the oxidation effect. In operating environment, the electrode potential generally fluctuates at an intermediate potential (0.6-1.1 V) [26]. Set electrode voltage:

$$u_{fc}\left(t\right) \in \left[0.6, 0.6 + \delta u\left(t\right)\right] \tag{24}$$

where u_{fc} is the electrode voltage, and δu represents the potential fluctuation value.

The decay rate rises as the upper limit potential $\delta u(t)$ grows, as predicted by the ECSA model. The objective of the strategy is to reduce volatility $\delta u(t)$.

Set the satisfaction index for voltage fluctuation:

$$S_u = -2\delta u\left(t\right) + 1 \tag{25}$$

From formula (25), when $\delta u(t)$ is 0.5 V, the satisfaction S_u is zero, indicating that the high potential is 1.1 V. When $\delta u(t)$ is zero, the satisfaction degree is 1.0. According to the test findings in Section III, when the upper level is 0.85 V, that is $\delta u(t)$ less than 0.25 V, the normalized ECSA remains 87% at the end of the period, suggesting that the ECSA decay rate is relatively slow, with S_u greater than 0.5.

The analysis of the voltage cycle reveals that extending the potential period is effective in delaying the ECSA's degradation. Consequently, it is advisable to extend the intervals between potential jumps to minimize frequent potential fluctuations caused by load variations.

Introduce the cycle satisfaction indicator. Section III reveals that attenuation is minimal when the square wave

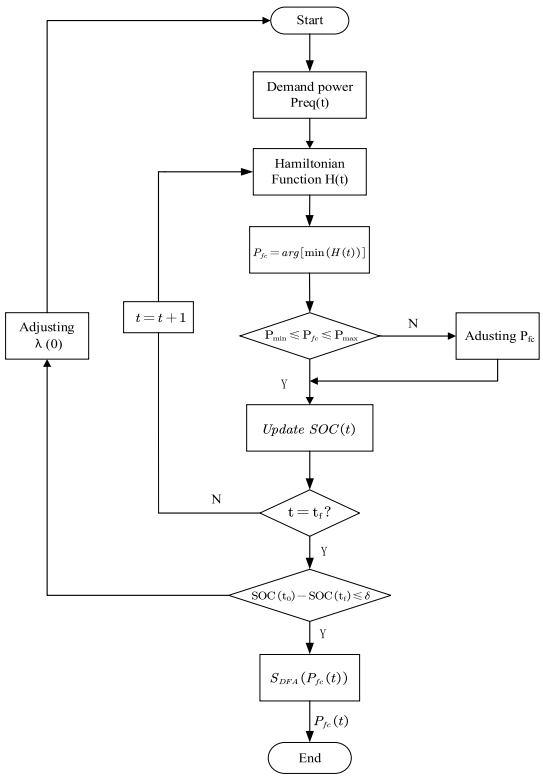

FIGURE 5. The algorithmic flow chart.

period exceeds 100 seconds, thus assigning a satisfaction degree of 1.0. Conversely, as the cycle period decreases, the satisfaction level correspondingly declines. The satisfaction is set as follows:

$$S_T = \frac{T}{99} - \frac{1}{99} \tag{26}$$

where S_T is the time cycle satisfaction index and T takes discrete values from 1 to 100 in steps of one second.

The aim is to enhance the satisfaction indicator S_T to increase the potential jump interval. The DC-AST test demonstrates that the decay rate of ECSA decay rate evidently slows down as T $\geq$ 20 seconds, that is $S_T \geq$19/99.

The ECSA decay rate is relatively slow when $\delta u(t)$ is less than 0.25 V and the satisfaction S_u is greater than 0.5. If the voltage satisfaction S_u is less than 0.5, it indicates a dramatic potential shift has occurred and the time should be recorded.

An adjustment function, designated as S_DFA, modulates P_{fc}(t) at each sampling point, guided by the satisfaction indices S_u and S_T. This function is characterized by three inputs: the initial power allocation denoted as P_{fc}, the set of satisfaction indices $S = \{S_u, S_T\}$, and the power at the optimal efficiency point, Pη. It then outputs an adjusted power allocation P'_{fc}. The following outlines the key steps involved in the design of S_DFA:

- *Step*1: Start a potential cycle, and initialize counter T
- *Step*2: Decision and adjust the power point
  - Adjust $P_{fc}(t)$ to P_η if $S_u(t) < 0.5$; otherwise, maintain current $P_{fc}(t)$
- *Step* 3: Counter Update
- Increment T ($T = T + 1$)
- *Step* 4: Periodic Satisfaction Check
- If $S_T \geq 19/99$ and $\delta u\left(t, P_{fc}\right) > 0.25$, start a new cycle and reset T
- *Step* 5: Sampling Point Update
- Increment t ($t = t + 1$)
- *Step* 6: Repeat steps 1$\sim$5

The hybrid strategy devised in this study is predicated upon the interaction and feedback of a two-layer model. Herein, the output of the upper-level PMP power allocation strategy serves as the input for the lower-level heuristic strategy, which further refines and adjusts the upper-level output.

- Initial optimization:

$$P_{fc}^{(0)}(t) = PMP\_Opt(t), t \in [1, N] \tag{27}$$

where $P_{fc}^{(0)}(t)$ denotes the power sequence optimized by the PMP algorithm after the initial iteration.

- Dynamic fluctuation regulation:

$$P_{fc}^{(n+1)}(t) = S\_DFA\left(P_{fc}^{(n)}(t), S\right), t \in [1, N] \tag{28}$$

Here, $P_{fc}^{(n)}(t)$ denotes the output power of the fuel cell at time t during the n^{th} iteration. The procedure involves refining the initial optimization results by implementing a dynamic fluctuation adjustment strategy, which is predicated on satisfaction indices.

In the strategy's upper layer, the PMP optimization algorithm is utilized to search for the global optimum with respect to the overall objective, while in the lower layer, heuristic rules are applied for fine-tuning, aiming to balance fuel economy and durability. Considering computational efficiency, a feedback iteration mechanism is not employed.

V. RESULTS AND DISCUSSION

Vehicle driving test cycles play a vital role in quantifying a vehicle's fuel consumption and emissions. In this section, we selected two representative test cycles, namely the China Light-duty Vehicle Test Cycle (CLTC) and the World Light Vehicle Test Cycle (WLTC), to evaluate fuel consumption and performance degradation. The energy management strategies are simulated in MATLAB/Simulink environment.

Previous research has rarely addressed the influence of a power splitting algorithm on fuel cell degradation. Leveraging the ECSA, this study provides a quantitative assessment of the impact of power splitting strategies on the performance degradation of PEMFCs.

A. PERFORMANCE EVALUATION UNDER CLTC DRIVING CYCLE

Fig. 6 illustrates the simulation results for fuel cell power, battery power, and SOC variation of the three strategies during

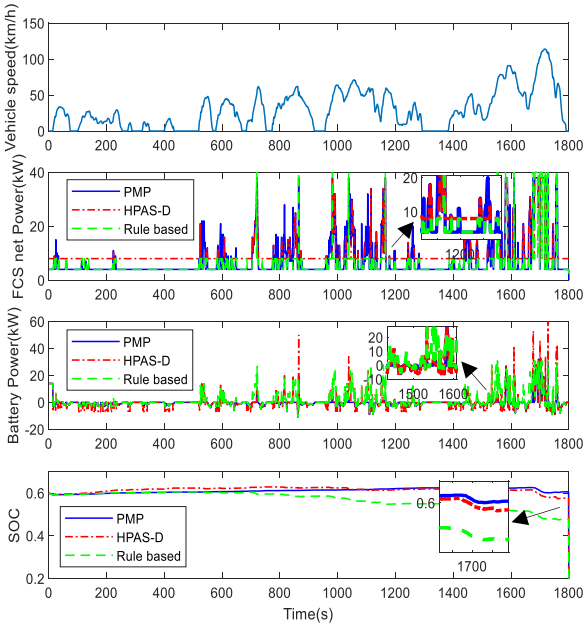

FIGURE 6. FC power, battery power, and SOC of the three strategies.

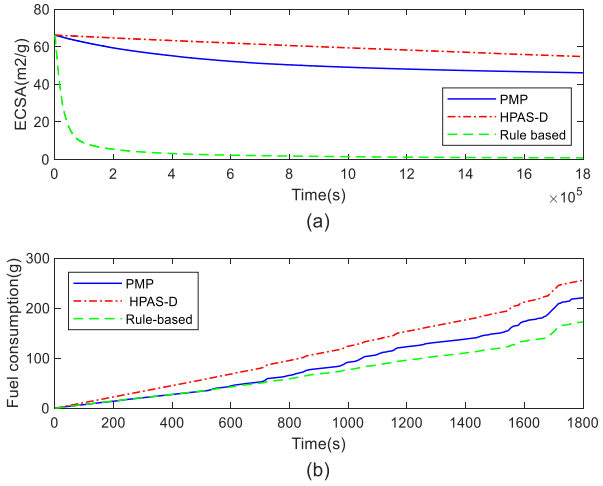

FIGURE 7. Comparison of three EMS on CLTC driving cycle: (a) ECSA decay of three strategies. (b). Fuel consumption.

the CLTC driving cycle. The initial battery SOC was set to 0.6.

As can be observed from the figure, under the HPAS-D strategy, although the output power of the fuel cell exhibits fluctuations, the peak magnitudes are much smaller, while the battery assuming a larger share of the load fluctuations. Additionally, under the HPAS-D strategy, the deviation of the final SOC relative to its initial value is minimized.

The algorithm demonstrates effective control over the battery's State of Charge (SOC), ensuring stable operation within a stable range. The fluctuation of the FC power based on the HPAS-D is relatively tiny during varying operating circumstances.

TABLE 3. ECSA decay and fuel consumption under three STRATEGIES.

CLTC	ECSA initial value	ECSA final value	$\Delta ECSA$ Percentage	Fuel consumption(g)
Rule based	66.2353	0.8500	98.72%	172.4763
PMP	66.2353	46.1792	30.28%	220.6773
HPAS-D	66.2353	54.8321	17.22%	255.6862

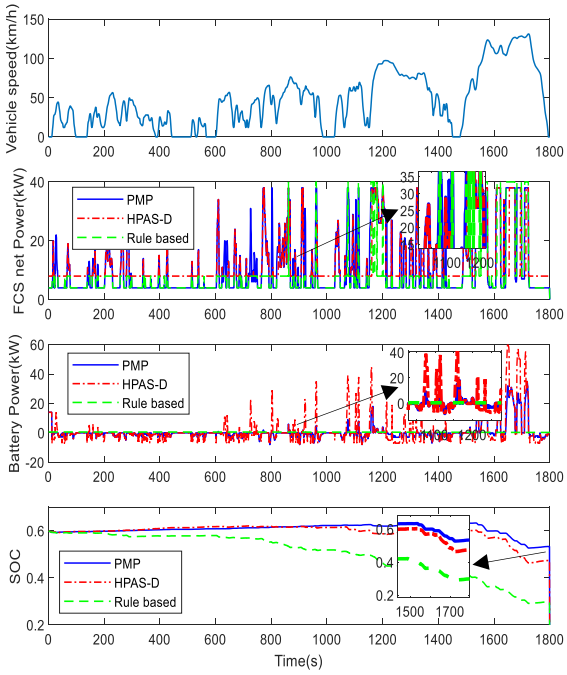

FIGURE 8. FC power, battery power and SOC of three strategies.

Convert the power signal into voltage and utilize it as input for the ECSA model to simulate 500 hours of operation. The ECSA change and fuel consumption of the three algorithms are shown in Fig. 7.

Table 3 details the specific values for ECSA changes and fuel consumption under the three strategies. After simulating uninterrupted operation for 500 hours under CLTC driving conditions, the ECSA under the rule-based strategy decreased from 66.2353 to 0.85, marking a substantial degradation of 98.72%. Notably, the HPAS-D strategy demonstrated the most effective delay in ECSA degradation, with only a 17.22% reduction, which is an 81.5% improvement over the rule-based approach. Compared to the classical PMP strategy, HPAS-D reduced ECSA degradation by 13.06%. However, there was a slight increase in fuel consumption. Detailed results are presented in Table 3.

B. PERFORMANCE EVALUATION UNDER WLTC DRIVING CYCLE

Compared to the NEDC, the WLTC test cycle exhibits more speed fluctuation and broader speed range coverage. The simulation results of three strategies are shown in Fig. 8, while Fig. 9 provides a comparison of ECSA variation and

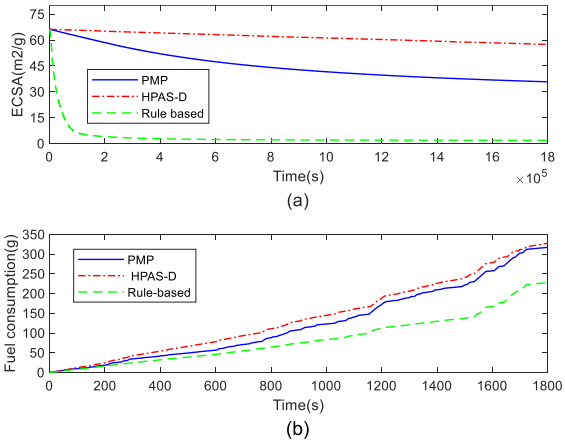

FIGURE 9. Comparison of three EMS under WLTC driving cycle: (a) ECSA decay for each strategy. (b). Fuel consumption for each strategy.

TABLE 4. ECSA decay and fuel consumption under three STRATEGIES.

WLTC	ECSA initial value	ECSA final value	$\Delta ECSA$ percentage	Fuel consumption(g)
Rule based	66.2353	1.9293	97.09%	227.8968
PMP	66.2353	35.8180	45.92%	317.2234
HPAS-D	66.2353	57.4766	13.22%	327.4486

fuel consumption among these strategies. The specific values of ECSA variations and fuel consumption after one drive cycle are listed in Table 4.

The data presented in Table 4 indicates that after a 500-hour simulation of uninterrupted operation under WLTC conditions, the ECSA drops from 66.2353 to 1.9293 in rule-based strategy with a 97.09% reduction. The PMP-based strategy results in a 45.92% decrease in ECSA. However, the HPAS-D strategy demonstrates a relatively minor decrease of 13.22%, which is an 83.87% improvement over the rule-based strategy. Contrasted with the PMP strategy, the degradation of ECSA is alleviated by 32.7%.

Fig. 6 to Fig. 9 and Tables 3-4 reveal that the HPAS-D strategy exhibits the slowest ECSA reduction across driving conditions. The rule-based strategy achieves the lowest fuel consumption, but it results in the most significant ECSA decline. Comparatively, while fuel consumption with the HPAS-D strategy marginally exceeds that of the PMP strategy, it notably slows down the rate of ECSA degradation.

Considering that the lower layer is based on heuristic rules, the iteration primarily focuses on the upper layer's PMP optimization strategy. Specifically, the process involves using a binary search method within a predefined search range to find the optimal co-state variable λ, until the preset convergence criteria are met. Given the driving conditions, the iterative process generally converges to the optimal λ value within a finite number of iterations. Through simulation tests, this strategy has been validated to be feasible in terms of convergence speed, stability under different initial conditions, and efficiency.

VI. CONCLUSION

This study presents an innovative energy management strategy aimed at addressing performance degradation in PEMFC vehicles. By developing an Electrochemical Active Surface Area (ECSA) model based on the platinum dissolution mechanism, and designing a dynamic condition accelerated stress test (DC-AST) that focuses on examining the effects of key parameters such as cycle period, amplitude, and duty cycle on the degradation of ECSA, the research elucidates the voltage characteristics pivotal to ECSA degradation. A heuristic strategy, based on the degradation characteristics, was developed for power adjustment. Subsequently, a composite strategy was constructed by integrating the heuristic approach with the classical PMP optimization. Simulation results indicate that, compared to traditional energy management strategies, the proposed strategy significantly reduces ECSA degradation during fuel cell operation. Under CLTC and WLTC typical operating conditions, ECSA degradation is diminished by 81.5% and 83.87%, respectively, compared to the rule-based strategy, and by 13.06% and 32.7%, respectively, compared to PMP optimization strategy. Notably, there is a slight increase in fuel consumption, while maintaining SOC fluctuations at a moderate level.

This study focuses on mitigating degradation in PEM fuel cells within HEVs, with emphasis on ECSA as a pivotal indicator of performance decline. A significant challenge lies in reducing fuel consumption while enhancing the durability of fuel cells. Future research will aim to optimize the balance between ECSA degradation and fuel consumption under varying driving conditions, with validation in actual systems.

REFERENCES

[1] Y. Manoharan, S. E. Hosseini, B. Butler, H. Alzhahrani, B. T. F. Senior, T. Ashuri, and J. Krohn, "Hydrogen fuel cell vehicles; current status and future prospect," *Appl. Sci.*, vol. 9, no. 11, p. 2296, Jun. 2019, doi: 10.3390/app9112296.

[2] P. Ren, P. Pei, Y. Li, Z. Wu, D. Chen, and S. Huang, "Degradation mechanisms of proton exchange membrane fuel cell under typical automotive operating conditions," *Prog. Energy Combustion Sci.*, vol. 80, Sep. 2020, Art. no. 100859, doi: 10.1016/j.pecs.2020.100859.

[3] K. Song, Y. Ding, X. Hu, H. Xu, Y. Wang, and J. Cao, "Degradation adaptive energy management strategy using fuel cell state-of-health for fuel economy improvement of hybrid electric vehicle," *Appl. Energy*, vol. 285, Mar. 2021, Art. no. 116413, doi: 10.1016/j.apenergy.2020.116413.

[4] A. Goshtasbi and T. Ersal, "Degradation-conscious control for enhanced lifetime of automotive polymer electrolyte membrane fuel cells," *J. Power Sources*, vol. 457, May 2020, Art. no. 227996, doi: 10.1016/j.jpowsour.2020.227996.

[5] Y. Zhou, H. Obeid, S. Laghrouche, M. Hilairet, and A. Djerdir, "A novel second-order sliding mode control of hybrid fuel cell/super capacitors power system considering the degradation of the fuel cell," *Energy Convers. Manage.*, vol. 229, Feb. 2021, Art. no. 113766, doi: 10.1016/j.enconman.2020.113766.

[6] Y. Feng and Z. Dong, "Optimal energy management strategy of fuel-cell battery hybrid electric mining truck to achieve minimum lifecycle operation costs," *Int. J. Energy Res.*, vol. 44, no. 13, pp. 10797–10808, Oct. 2020, doi: 10.1002/er.5728.

[7] H. Li, A. Ravey, A. N'Diaye, and A. Djerdir, "Online adaptive equivalent consumption minimization strategy for fuel cell hybrid electric vehicle considering power sources degradation," *Energy Convers. Manage.*, vol. 192, pp. 133–149, Jul. 2019, doi: 10.1016/j.enconman.2019.03.090.

[8] L. Kwon, D.-S. Cho, and C. Ahn, "Degradation-conscious equivalent consumption minimization strategy for a fuel cell hybrid system," *Energies*, vol. 14, no. 13, p. 3810, Jun. 2021, doi: 10.3390/en14133810.
[9] T. Li, H. Liu, H. Wang, and Y. Yao, "Multiobjective optimal predictive energy management for fuel cell/battery hybrid construction vehicles," *IEEE Access*, vol. 8, pp. 25927–25937, 2020, doi: 10.1109/ACCESS.2020.2969494.
[10] Y. Zhou, A. Ravey, and M.-C. Péra, "Real-time cost-minimization power-allocating strategy via model predictive control for fuel cell hybrid electric vehicles," *Energy Convers. Manage.*, vol. 229, Feb. 2021, Art. no. 113721, doi: 10.1016/j.enconman.2020.113721.
[11] H. He, S. Quan, F. Sun, and Y.-X. Wang, "Model predictive control with lifetime constraints based energy management strategy for proton exchange membrane fuel cell hybrid power systems," *IEEE Trans. Ind. Electron.*, vol. 67, no. 10, pp. 9012–9023, Oct. 2020.
[12] K. Fu, T. Tian, Y. Chen, S. Li, C. Cai, Y. Zhang, W. Guo, and M. Pan, "The durability investigation of a 10-cell metal bipolar plate proton exchange membrane fuel cell stack," *Int. J. Energy Res.*, vol. 43, no. 7, pp. 2605–2614, Jun. 2019, doi: 10.1002/er.4283.
[13] J. Fu, L. Zeng, J. Lei, Z. Deng, X. Fu, X. Li, and Y. Wang, "A real-time load prediction control for fuel cell hybrid vehicle," *Energies*, vol. 15, no. 10, p. 3700, May 2022, doi: 10.3390/en15103700.
[14] S. Cherevko, G. P. Keeley, S. Geiger, A. R. Zeradjanin, N. Hodnik, N. Kulyk, and K. J. J. Mayrhofer, "Dissolution of platinum in the operational range of fuel cells," *ChemElectroChem*, vol. 2, no. 10, pp. 1471–1478, Oct. 2015, doi: 10.1002/celc.201500098.
[15] T. Jahnke et al., "Performance and degradation of proton exchange membrane fuel cells: State of the art in modeling from atomistic to system scale," *J. Power Sources*, vol. 304, pp. 207–233, Feb. 2016, doi: 10.1016/j.jpowsour.2015.11.041.
[16] R. Borup et al., "Scientific aspects of polymer electrolyte fuel cell durability and degradation," *Chem. Rev.*, vol. 107, no. 10, pp. 3904–3951, Oct. 2007, doi: 10.1021/cr0501821.
[17] S. Stariha, N. Macauley, B. T. Sneed, D. Langlois, K. L. More, R. Mukundan, and R. L. Borup, "Recent advances in catalyst accelerated stress tests for polymer electrolyte membrane fuel cells," *J. Electrochem. Soc.*, vol. 165, no. 7, pp. 492–501, 2018, doi: 10.1149/2.0881807jes.
[18] M. Zhao, W. Shi, B. Wu, W. Liu, J. Liu, D. Xing, Y. Yao, Z. Hou, P. Ming, J. Gu, and Z. Zou, "Analysis of carbon-supported platinum through potential cycling and potential-static holding," *Int. J. Hydrogen Energy*, vol. 39, no. 25, pp. 13725–13737, Aug. 2014.
[19] S. G. Rinaldo, J. Stumper, and M. Eikerling, "Physical theory of platinum nanoparticle dissolution in polymer electrolyte fuel cells," *J. Phys. Chem. C*, vol. 114, no. 13, pp. 5773–5785, Apr. 2010, doi: 10.1021/jp9101509.
[20] W. Bi and T. F. Fuller, "Modeling of PEM fuel cell Pt/C catalyst degradation," *J. Power Sources*, vol. 178, no. 1, pp. 188–196, Mar. 2008, doi: 10.1016/j.jpowsour.2007.12.007.
[21] F. Hiraoka, Y. Kohno, K. Matsuzawa, and S. Mitsushima, "A simulation study of Pt particle degradation during potential cycling using a dissolution/deposition model," *Electrocatalysis*, vol. 6, no. 1, pp. 102–108, Jan. 2015, doi: 10.1007/s12678-014-0225-y.
[22] D. J. S. Sandbeck, M. Inaba, J. Quinson, J. Bucher, A. Zana, M. Arenz, and S. Cherevko, "Particle size effect on platinum dissolution: Practical considerations for fuel cells," *ACS Appl. Mater. Interface*, vol. 12, no. 23, pp. 25718–25727, Jun. 2020.
[23] J. C. Meier, C. Galeano, I. Katsounaros, J. Witte, H. J. Bongard, A. A. Topalov, C. Baldizzone, S. Mezzavilla, F. Schüth, and K. J. J. Mayrhofer, "Design criteria for stable Pt/C fuel cell catalysts," *Beilstein J. Nanotechnol.*, vol. 5, pp. 44–67, Jan. 2014, doi: 10.3762/bjnano.5.5.
[24] H. Yano, M. Watanabe, A. Iiyama, and H. Uchida, "Particle-size effect of Pt cathode catalysts on durability in fuel cells," *Nano Energy*, vol. 29, pp. 323–333, Nov. 2016, doi: 10.1016/j.nanoen.2016.02.016.
[25] R. M. Darling and J. P. Meyers, "Kinetic model of platinum dissolution in PEMFCs," *J. Electrochemical Soc.*, vol. 150, no. 11, p. A1523, 2003, doi: 10.1149/1.1613669.
[26] Y. Fan, "Design of used range of battery SOC for hybrid EV," *Automot. Elect. Parts*, vol. 56, no. 6, pp. 153–156, 2015.
[27] X. Li, Y. Wang, D. Yang, and Z. Chen, "Adaptive energy management strategy for fuel cell/battery hybrid vehicles using Pontryagin's minimal principle," *J. Power Sources*, vol. 440, Nov. 2019, Art. no. 227105.
[28] X. Meng, Q. Li, W. Chen, and G. Zhang, "An energy management method based on Pontryagin minimum principle satisfactory optimization for fuel cell hybrid systems," *Proc. CSEE*, vol. 39, no. 3, pp. 782–792, 2019.

JUN FU was born in Hubei, China. He received the M.S. degree in control theory and control engineering from Wuhan University of Science and Technology, Wuhan, China, in 2007. He is currently pursuing the Ph.D. degree in control science and engineering with Huazhong University of Science and Technology, Wuhan.

He was with Wuhan Boyu Optoelectronics Company Ltd., from 2007 to 2008, and Jingchu Institute of Technology, from 2009 to 2018. His main research interests include fuel cell modeling and optimal control and energy management strategies for hybrid power systems.

QIAN XIANG was born in 1997. He is from Guizhou, China. He received the master's degree in aerospace engineering from Beijing Institute of Technology, in 2022. He is currently pursuing the Ph.D. degree with the School of Artificial Intelligence and Automation, Huazhong University of Science and Technology.

His research interests include fuel cell consistency and homogeneity problems and optimal control strategy design for hybrid power systems.

LINGHONG ZENG received the B.S. degree in automation from North China Electric Power University, Beijing, China, in 2021. He is currently pursuing the Ph.D. degree in control science and engineering with the School of Artificial Intelligence and Automation, Huazhong University of Science and Technology, Wuhan, China. His main research interest includes energy management of PEM fuel cell hybrid energy systems.

YANMIN ZU was born in Hebei, China, in 1995. She received the M.S. degree from the School of Artificial Intelligence and Automation, Huazhong University of Science and Technology, Wuhan, in 2022.

Her research in PEM performance degradation and hybridization with Huazhong University of Science and Technology. She is currently with State Grid Corporation, Beijing, China. Her main research interests include fuel cell system modeling and simulation and PEM electrolysis for hydrogen production.

HANG YOU was born in Tianmen, Hubei, in 1997. He received the B.S. and M.S. degrees from the School of Artificial Intelligence and Automation, Huazhong University of Science and Technology, Wuhan, China, in 2018 and 2021, respectively.

He is currently with Weimax New Energy Company, Shenzhen. His main research interests include fuel cell system modeling and controller embedded software development.

XINKAI SHAN received the B.S. degree in electrical engineering and its automation from Zhengzhou University, Henan, China, in 2022. He is currently pursuing the master's degree in control science and engineering with the School of Artificial Intelligence and Automation, Huazhong University of Science and Technology, Wuhan, China.

His research interests include energy management strategy for fuel cell hybrid power systems and extending the service life of fuel cell.

JIE XIN was born in 1997. He is from Anhui, China. He received the bachelor's degree in artificial intelligence and automation from Anhui University of Science and Technology, Anhui, China, in 2018, and the master's degree from Huazhong University of Science and Technology, Wuhan, China, in 2020.

He is currently with ArcSoft, Hangzhou. His main research interests include battery energy management strategy and the degression of fuel cell.

XI LI (Member, IEEE) received the Ph.D. degree in engineering from the Department of Automation, Shanghai Jiao Tong University, Shanghai, China, in 2005.

He was a Visiting Scholar with the University of Michigan, Ann Arbor, USA, in 2011. He is currently a Full Professor with the School of Artificial Intelligence and Automation, Huazhong University of Science and Technology. His research interests include smart energy, hydrogen energy and fuel cells, and micro-energy network control.

Prof. Li serves as a Responsible Expert for Science and Technology Projects at the Headquarters of the State Grid Corporation of China, a member of the Vehicle Control and Intelligence Professional Committee of Chinese Society of Automation, and a member of the National Energy Industry High Temperature Fuel Cell Standards Committee. He is a member of IEEE PES Energy Storage Technical Committee (China) Hydrogen Energy Storage Technology Sub-Committee.